Calibration Study of Continuously Controllable Output Characteristics of Magnetorheological Suspension

Xin-feng Ge, Wen-feng Li, Man-ying Liang, Shen-shen Zhang, Kai-yang Huo

Abstract—**To thoroughly examine the output characteristics of a semi-active vehicle suspension system featuring a magneto-rheological (MR) damper, a filtered white noise method and a first-order Padé approximation are used to model the random road excitation affecting the front and rear wheels. The rheological properties of the selected MR fluid are carefully analyzed, and a double-ended MR damper is developed based on these properties. This process involves the design, fabrication, and testing of the MR damper, followed by the development of a control model informed by the experimental results. A four-degree-of-freedom (4-DOF) dynamic model of the MR semi-active vehicle suspension, incorporating the double-ended MR damper, is established for both the front and rear wheels. Numerical simulations are performed to assess the impact of vehicle speed and MR damper excitation current on the suspension system's output response. The results show that variations in vehicle speed and MR damper excitation current significantly affect the suspension's output characteristics. Additionally, the suspension's output characteristics vary consistently with changes in vehicle speed and MR damper excitation current, indicating excellent controllability.**

Index Terms—**double-ended MR damper, first-order Padé approximation method, output characteristics, 4-DOF MR semi-active suspension, dynamics mode**

I. Introduction

As the economy and society continue to develop, automobiles have become an essential mode of transportation in daily life and work. Simultaneously, there has been a substantial rise in the demand for enhanced ride comfort and improved handling stability in vehicles [1-3]. The suspension system is a crucial element of modern automobiles, playing a critical role in influencing both ride comfort and handling stability [4]. Designing an intelligent suspension system that can adjust in real-time based on road conditions and vehicle status is a promising way to improve ride comfort, safety, and stability [5]. MR dampers provide real-time adjustability of damping characteristics [6]. Semi-active suspensions using MR dampers are known for their excellent controllability, broad dynamic range, rapid response, and low energy consumption. These features have made MR-based semi-active suspensions a leading area of research and development in intelligent suspension systems [7-10].

Developing, testing, and modeling MR dampers for vehicles, along with investigating the impact of MR damper output force on suspension performance, are critical technologies for advancing MR suspension systems [11]. This study explores the dynamic characteristics of designed MR dampers and MR semi-active suspensions through theoretical analysis, performance testing, control modeling, and numerical simulation. These approaches provide a comprehensive theoretical basis for evaluating, improving, and optimizing MR dampers and MR semi-active suspension systems for vehicles.

II. Road Random Excitation Model

A. Front wheel road excitation

The filtered white noise method represents the random road excitation acting on the front wheel. The corresponding equation is shown below [12].

$$\dot{q}_f(t) = -2\pi n_q u q_f(t) + 2\pi n_0 \sqrt{G_q(n_0)u}\, w(t) \qquad (1)$$

Here, $q_f(t)$ represents the front wheel road excitation, $w(t)$ denotes ideal white noise, and u is the vehicle speed; n_0 refers to the reference frequency, with a value of n_0 =0.1 m^{-1}, $G_q(n_0)$ represents the road surface roughness coefficient, provided by the standard. n_q is the lower cut-off frequency, set as n_q =0.0001 m^{-1} here, ensuring that the root mean square value of the road excitation power spectral density closely matches the value specified by the national standard [13,14].

B. Rear wheel road excitation

Assuming the vehicle moves in a straight path on a rigid road surface, the input trajectories of the front and rear wheels can be considered to have a specific time lag [15]. This relationship is given as follows.

Manuscript received April 25, 2024; revised October 22, 2024.

This work was financially supported by the Natural Science Foundation of Henan Province, China (No. 242300420049), the National College Student Innovation and Entrepreneurship Training Program, China (No. 202310480006).

Xin-feng Ge is a professor of School of Electrical and Mechanical Engineering, Xuchang University, Xuchang, 461000, China.(corresponding author, phone:+8618539037370; e-mail: gexf@xcu.edu.cn)

Wen-feng Li is a lecturer of School of Electrical and Mechanical Engineering, Xuchang University, Xuchang, 461000, China. (e-mail: 418974195@qq.com)

Man-ying Liang is a lecturer of School of Electrical and Mechanical Engineering, Xuchang University, Xuchang, 461000, China. (e-mail: 1324981596@qq.com)

Shen-shen Zhang is an undergraduate student of School of Electrical and Mechanical Engineering, Xuchang University, Xuchang, 461000, China. (e-mail: 2073931517@qq.com)

Kai-yang Huo is an undergraduate student of School of Electrical and Mechanical Engineering, Xuchang University, Xuchang, 461000, China. (e-mail: 1468523752@qq.com)

$$q_r(t) = q_f(t - t_d) \quad (2)$$

Here, q_f and q_r denote the road excitations for the front and rear wheels, respectively; t_d is the lag time between the road excitations of the front and rear wheels; $t_d = L/u$, where L and u are the wheelbase and the vehicle speed.

Applying the Laplace transform to Equation (2) yields Equation (3) [16].

$$\frac{q_r(s)}{q_f(s)} = e^{-st_d} \quad (3)$$

Here, s is the frequency; $q_r(s)$ and $q_f(s)$ denote the Laplace transform of $q_r(t)$ and $q_f(t)$.

In this context, the first-order Padé approximation [17] is used to approximate the correlation between the front and rear wheels described in Equation (3). As a result, the road excitation for the rear wheels is derived, as shown in Equations (4) and (5).

$$\dot{x} = -\frac{2}{t_d}x + \frac{2}{t_d}q_f(t) \quad (4)$$

$$q_r(t) = 2x - q_f(t) \quad (5)$$

Here, x represents an intermediate state variable.

C. Time-domain model and simulation of road random excitation on front and rear wheel

Time-domain models of road random excitation for the front and rear wheels are developed using Equations (1) and (4)-(5). A numerical simulation model is then constructed using MATLAB/Simulink, as shown in Figure 1.

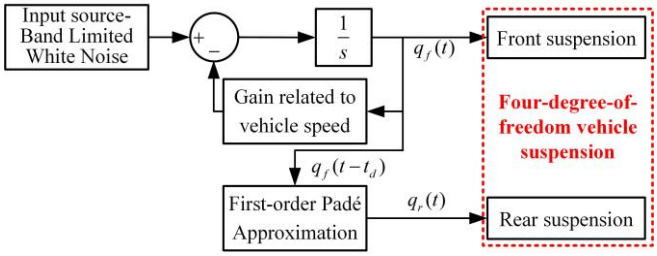

Fig. 1. Simulink model for the excitation of front and rear wheels due to road surface conditions

The parameters for the time-domain model of road random excitation are as follows: B-level road surface, varying speed conditions, a wheelbase of 2.76 meters, a simulation duration of 10 seconds, and a sampling interval of 0.005 seconds. Numerical simulation of the time-domain model yields the time-domain curves of road random excitation for the front and rear wheels, as shown in Figure 2.

The power spectral density (PSD) curve of road random excitation is obtained by applying the pwelch method [18] to the time-domain curve at a speed of 40 km/h. The resulting PSD curve is displayed in Figure 3.

Figure 3 shows that the PSD curves for the front and rear wheel road random excitation models, based on filtered white noise, mostly fall within the standard B-level road PSD. Additionally, these curves are evenly distributed around the average PSD of the standard B-level road. This confirms the accuracy and applicability of the developed front and rear wheel road excitation models and the corresponding numerical simulation models.

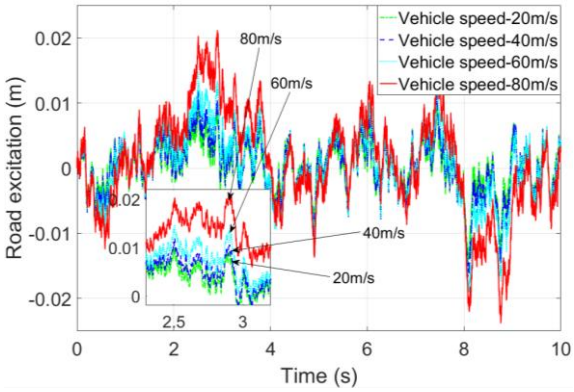

(a) Front wheel road excitation at different speed

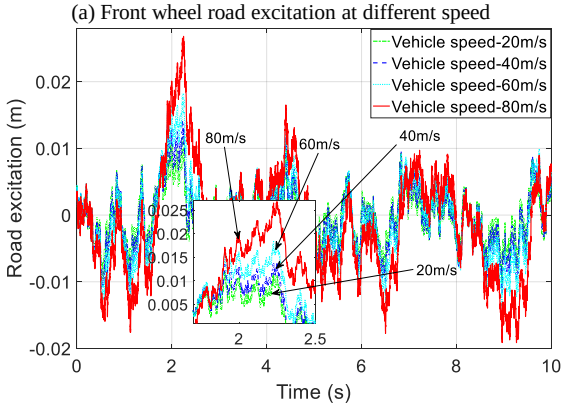

(b) Rear wheel road excitation at different speed

Fig.2. Time domain numerical simulation curves under the front and rear wheels road random excitation

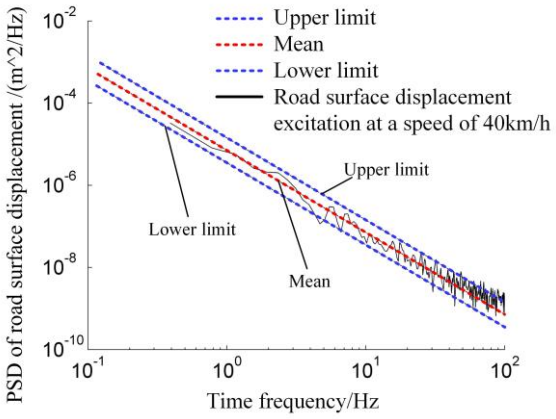

(a) PSD of the front wheel road random excitation

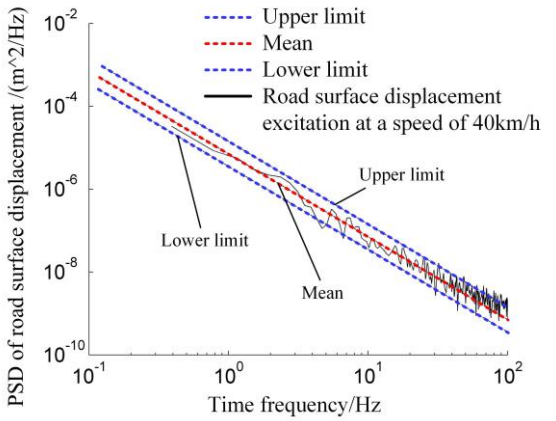

(b) PSD of the rear wheel road random excitation

Fig.3. PSD curves of road random excitation of front and rear wheels at 40 km/h speed

III. Double-Ended Rod Magneto Rheological Damper for Vehicles

MR fluid is an advanced smart material with tunable rheological properties [19]. By utilizing the tunable properties of MR fluid, the designed MR damper operates as a semi-active actuator with continuously adjustable damping. This damper provides several advantages, including a simple structure, low energy usage, a broad dynamic range, rapid response, and adjustable damping [20].

A. Rheological properties of MR fluids

An MR fluid, developed by a domestic research institute [21], was tested using the rheometer system shown in Figure 4. The test conditions included magnetic induction intensities ranging from 0 T to 0.75 T, and shear rates from 0 to 100 s^{-1}. The resulting shear stress-shear rate curves for the MR fluid are presented in Figure 5.

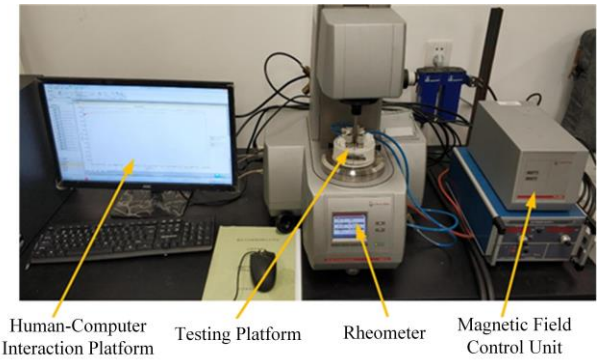

Fig.4. Rheometer test system

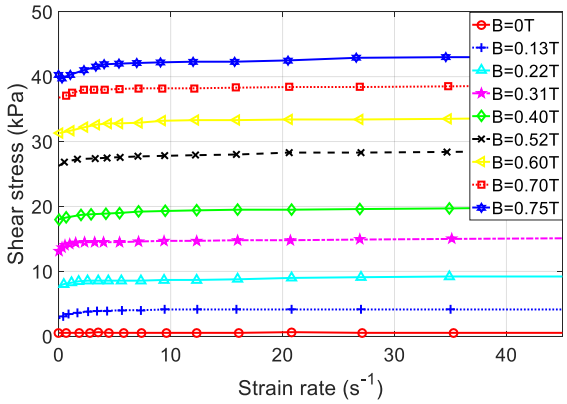

Fig.5. Shear stress-shear rate curves for magneto rheological fluids

Except for the low shear rate region at the initial stage, the slope of the shear stress-shear rate curves under different magnetic field intensities is negligible. This suggests that the zero-field viscosity of the MR fluid is very low, which benefits the optimization of MR damper output characteristics. As the magnetic field intensity increases from 0 T to 0.75 T, the MR fluid's shear stress rises from approximately 0.02 kPa to around 45 kPa. This demonstrates that the selected MR fluid has a broad rheological adjustment range under different magnetic field intensities, making it an effective force transfer medium for MR dampers.

B. Design of Double-Ended Rod Magneto rheological damper

A double-ended rod MR damper operating in shear mode [22] is proposed based on the output characteristics and spatial structure of vehicle dampers, with a focus on structural simplification and coaxiality optimization, as shown in Figure 6. The damper consists of a cylinder, piston, upper and lower piston rods, guide ring, oil seal, positioning ring, guide seat, end cover, MR fluid in the working chamber, a spring seat for damper springs, and non-spring-loaded masses like the bracket plate for connecting tires.

The external dimensions, working stroke, installation method, and size of the double-ended rod MR damper are compatible with the passive damper of a small car in China to ensure interchangeability. A prototype based on this structure has been developed, as shown in Figure 7.

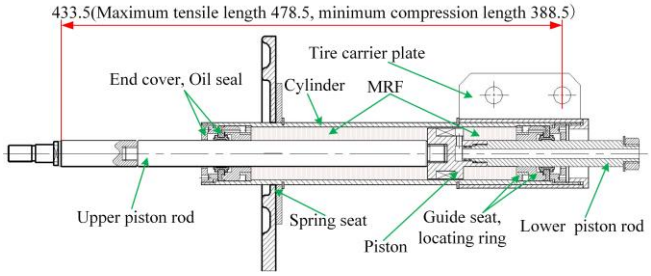

Fig.6 Structure of double-ended MR damper

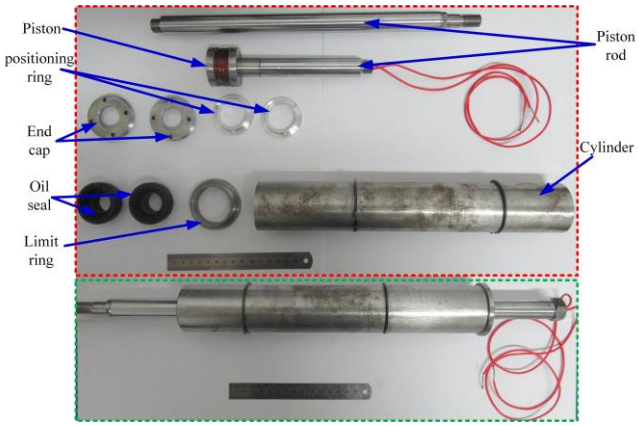

Fig.7. Assembly and prototype of double-ended MR damper

C. Output characteristics of MR damper

To assess the applicability of the double-ended rod MR damper, experiments were conducted following the national test standard QC/T 545-1999 [23, 24] for vehicle dampers, as shown in Figure 8.

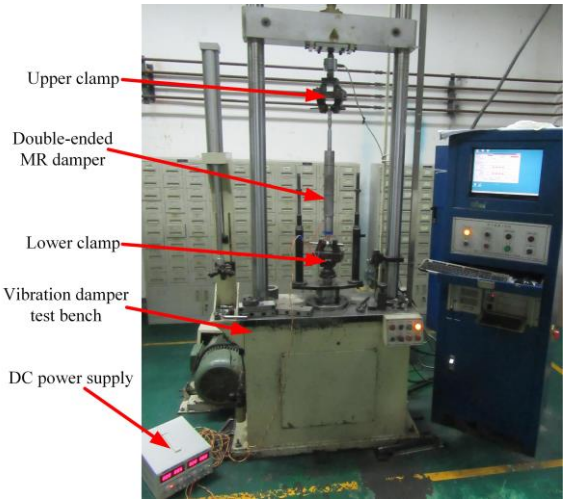

Fig.8. Test setup for double-ended MR damper

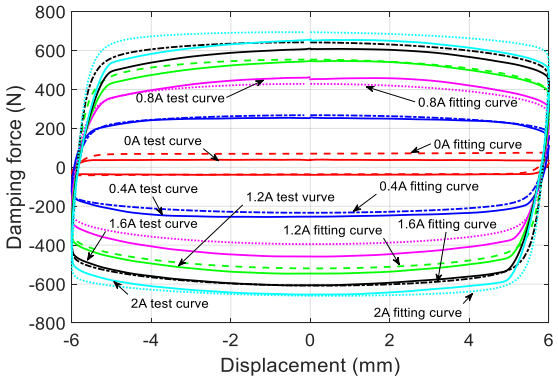

(a) Damping force-displacement curves under 6 mm and 0.6 Hz

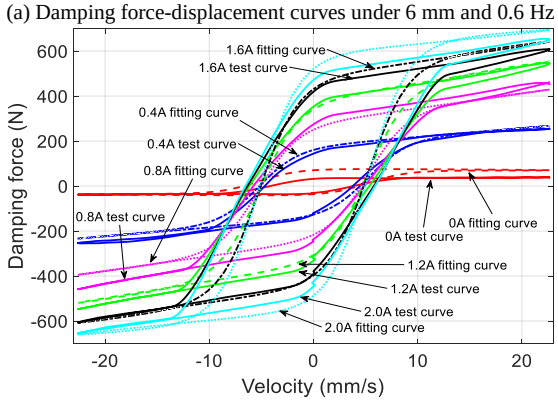

(b) Damping force -velocity curves under 6 mm and 0.6 Hz

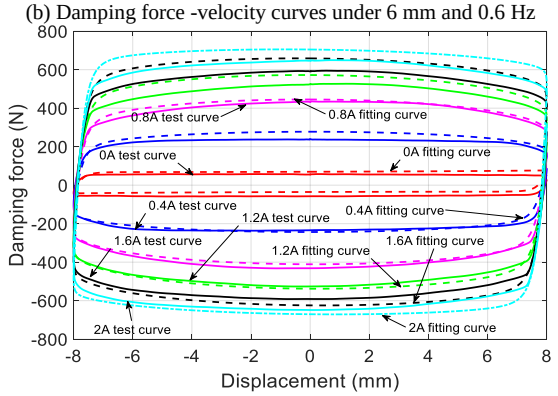

(c) Damping force-displacement curves under 8 mm and 0.5 Hz

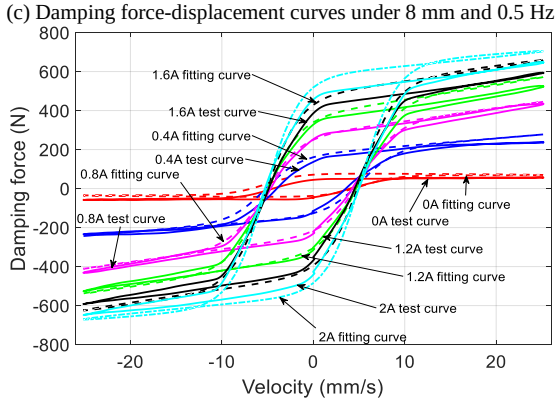

(d) Damping force -velocity curves under 8 mm and 0.5 Hz

Fig.9. Comparison between model and test results (Solid line-test result, dashed line-identified line)

The MR damper was mounted on an electro-hydraulic servo testing machine with an integrated sensing and excitation loading system. A DC stabilized power supply was used to power the MR damper coil.

The damper's output damping characteristics were tested under varying excitation currents and sinusoidal frequencies. The test conditions were:

Excitation amplitude: ± 6 mm, ± 8 mm, ± 10 mm

Excitation frequency: 0.4 Hz, 0.5 Hz, 0.6 Hz

Excitation current: 0 A to 2.0 A in 0.2 A increments.

For each condition, 5-10 cycles were recorded to obtain stable raw data for the indicator curve. The current was gradually increased from 0 A to 2.0 A, with varying sinusoidal excitation frequencies and amplitudes. The output characteristics of the double-ended rod MR damper were obtained under varying excitation conditions and currents.

Figure 9 shows the output characteristic curves at different excitation currents, with amplitudes of 6 mm and 8 mm and frequencies of 0.5 Hz and 0.6 Hz. As the excitation current increases, the MR damper's output damping force also rises, as indicated by the expanding envelope of the energy dissipation curve. At constant piston speed, increasing the excitation current leads to a proportional rise in output damping force. When the excitation current increases from 1.2 A to 2.0 A, the damping force peak shows a slight attenuation trend. This suggests that as excitation current increases, the magnetic induction generated by the piston coil in the working area gradually approaches saturation. Beyond this point, further increases in excitation current lead to diminishing gains in output damping force until the magnetic field is fully saturated.

The damper's output damping force remains largely unaffected by different excitation amplitudes, suggesting that amplitude has minimal impact on the performance of the double-ended rod MR damper.

D. Modeling of MR damper

The indicator and speed-force curves of the MR damper show that its output damping force is simultaneously affected by piston displacement, speed, and excitation current. After analyzing the output curves and comparing the attributes of various damper models, the hyperbolic tangent model was chosen to accurately represent the double-ended rod MR damper.

The hyperbolic tangent model is straightforward, facilitates easy parameter identification, and delivers high accuracy in modeling. The model is expressed as follows:

$$F = c\dot{x} + kx + \alpha \tanh(\beta\dot{x} + \delta sign(x)) + f_0 \qquad (6)$$

Here, $c = g_1 I^2 + g_2 I + g_3, k = g_4 I + g_5, \alpha = g_6 I + g_7$

The hyperbolic tangent model was fitted using experimental data from the damper at 6 mm excitation amplitude and 0.6 Hz frequency under various excitation currents. The parameters identified for the model are shown in Table 1.

TABLE I
HYPERBOLIC TANGENT MODEL PARAMETERS OF DOUBLE-ENDED MR DAMPER

Fitting coefficient	Value
g_1	-5.098
g_2	10.17
g_3	0.6561
g_4	-1.306
g_5	0.5209
g_6	277.5
g_7	48.86
β	0.4055
δ	1.3137
f_0	18.91

A comparison between the hyperbolic tangent model and experimental data, as shown in Figure 9, reveals that the fitted curve aligns closely with the experimental curve, with only minor deviations at certain excitation currents. This indicates that the hyperbolic tangent model effectively captures the hysteresis behavior of the double-ended rod MR damper.

IV. Four DOF (Degree of Freedom) Vehicle Suspension Model

A. Establishment of a 4 DOF vehicle suspension model

To develop a 4-DOF vehicle suspension model for the front and rear wheels, the following assumptions are made [25]:

a) The inputs to the vehicle's left and right wheels are assumed identical, with the vehicle's geometric dimensions and mass distribution symmetrical, leading to identical motion on both sides.

b) The vehicle body is simplified as a rigid body that can undergo vertical and pitch motion, while the un-sprung mass is simplified as a rigid body limited to vertical motion.

c) Tire damping is neglected, and the tire is simplified as a linear spring, while the suspension is modeled as a combination of linear springs and dampers.

d) The assumption is that the road excitation point is consistently situated at the center of the contact area between the tire and the pavement.

Based on these assumptions, a 4-DOF vehicle suspension model is developed to represent the front and rear wheels, as shown in Figure 10. The model includes the suspension's spring-loaded mass, two damper assembly systems linking the front and rear wheels to the suspension, the un-sprung mass, and the tire stiffness of the front and rear wheels.

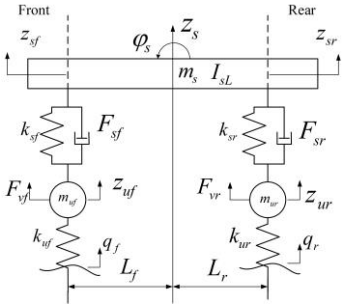

Fig.10. 4-DOF model of vehicle suspension

Figure 10 shows a 4-DOF half-vehicle suspension model, which includes the front and rear wheels. Table 2 lists the definitions and values for all parameters.

From Figure 10, the dynamic equations for the vehicle suspension, represented by Equations (7) to (10), are derived.

$$m_s\ddot{z}_s = -k_{sf}(z_{sf}-z_{uf}) + F_{sf} - k_{sr}(z_{sr}-z_{ur}) + F_{sr} \quad (7)$$

$$I_{sL}\ddot{\phi}_s = L_f[k_{sf}(z_{sf}-z_{uf}) - F_{sf}] - L_r[k_{sr}(z_{sr}-z_{ur}) - F_{sr}] \quad (8)$$

$$m_{uf}\ddot{z}_{uf} = -k_{uf}(z_{uf}-q_f) - F_{sf} + k_{sf}(z_{sf}-z_{uf}) \quad (9)$$

$$m_{ur}\ddot{z}_{ur} = -k_{ur}(z_{ur}-q_r) - F_{sr} + k_{sr}(z_{sr}-z_{ur}) \quad (10)$$

Equations (7) to (10) can be rewritten as follows.

$$[M]\{\ddot{z}\} + [C]\{F_s\} + [K]\{z\} = [K_u]\{q\} \quad (11)$$

Here,

$$\{z\} = \{z_{uf} \quad z_{ur} \quad z_s \quad \phi_s\}^T, \{q\} = \{q_f \quad q_r\}^T,$$

$$[M] = diag[m_{uf} \quad m_{ur} \quad m_s \quad I_{sL}], [C] = \begin{bmatrix} 1 & 0 \\ 0 & 1 \\ -1 & -1 \\ L_f & -L_r \end{bmatrix},$$

$$[K] = \begin{bmatrix} k_{uf}+k_{sf} & 0 & -k_{sf} & L_f k_{sf} \\ & k_{ur}+k_{sr} & -k_{sr} & -L_r k_{sr} \\ & & k_{sf}+k_{sr} & L_r k_{sr} - L_f k_{sf} \\ & \text{symmetry} & & L_f^2 k_{sf} + L_r^2 k_{sr} \end{bmatrix},$$

$$\{F_s\} = \{F_{sf} \quad F_{sr}\}, [K_u] = \begin{bmatrix} k_{uf} & 0 \\ 0 & k_{ur} \\ 0 & 0 \\ 0 & 0 \end{bmatrix}.$$

TABLE II
Parameters Indication of the Vehicle Suspension Model

Parameter	Meaning	Value/Unit
m_s	sprung mass	372.6 kg
I_{sL}	Vehicle pitch inertia moment	384.4 kgm^2
m_{uf}	Front axle un-sprung mass	25.35 kg
m_{ur}	Rear axle un-sprung mass	68.8 kg
k_{uf}	Front tire stiffness	181 kN/m
k_{ur}	Rear tire stiffness	181 kN/m
k_{sf}	Front suspension stiffness	30 kN/m
k_{sr}	Rear suspension stiffness	30 kN/m
F_{sf}	Front suspension damping force	N
F_{sr}	Rear suspension damping force	N
L_f	Distance between front axle and mass center	1.1161 m
L_r	Distance between rear axle and mass center	1.2319 m
z_s	Mass center vertical displacement	m
φ_s	Mass center Pitch angle	rad
z_{uf}	Vertical displacement of un-sprung loaded mass on the front axle	m
z_{ur}	Vertical displacement of un-sprung loaded mass on the rear axle	m
q_f	Front wheel road excitation	m
q_r	Rear wheel road excitation	m

B. Modeling simulation platform for MR vehicle suspension

A simulation platform for a 4-DOF vehicle suspension model is developed in MATLAB/Simulink using Equations (6) to (11), as illustrated in Figure 11.

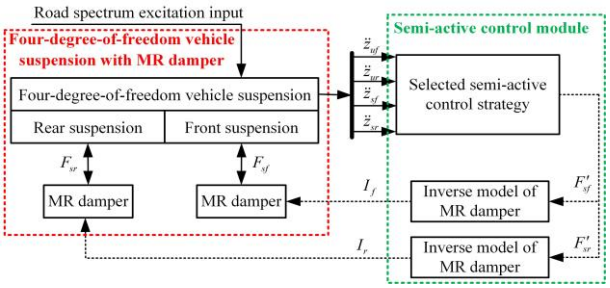

Fig.11. Simulink model of 4-DOF model

V. Simulation Results Analysis

A. Simulation Analysis Scheme

The evaluation of the vehicle suspension performance with the double-ended rod MR damper involves measuring the vertical acceleration of the sprung mass, the pitch angle acceleration of the vehicle, suspension deflection at both the front and rear, and the dynamic load on the front and rear tires. The root mean square (RMS) values from time-domain simulation data under various road conditions are used as evaluation metrics. The output characteristics of the MR suspension are analyzed from both longitudinal and transverse perspectives.

(a) **Longitudinal Analysis:** With suspension parameters constant, the vehicle speed is varied from 5 km/h to 80 km/h in 5 km/h increments. The analysis examines the effect of speed on the suspension's response.

(b) **Transverse Analysis:** With all other parameters unchanged, the MR damper excitation current is increased from 0 A to 2.0 A. The analysis evaluates the impact of excitation current (damping) on the suspension's output response.

B. Simulation Results

Simulation parameters are set based on the simulation scheme, including a B-level road grade and a simulation time corresponding to the vehicle's travel over 200 meters at a specified speed, with a 0.005-second sampling interval.

Figure 12 displays the results, from which the following conclusions are drawn:

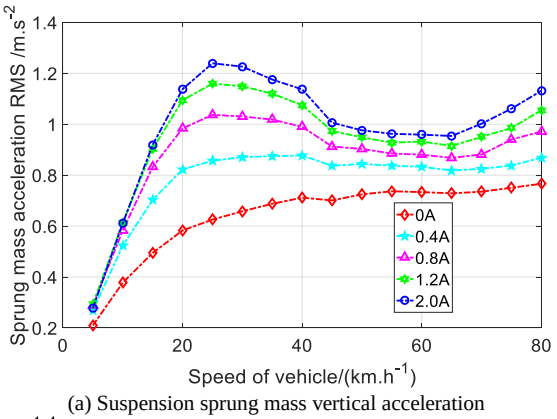

(a) Suspension sprung mass vertical acceleration

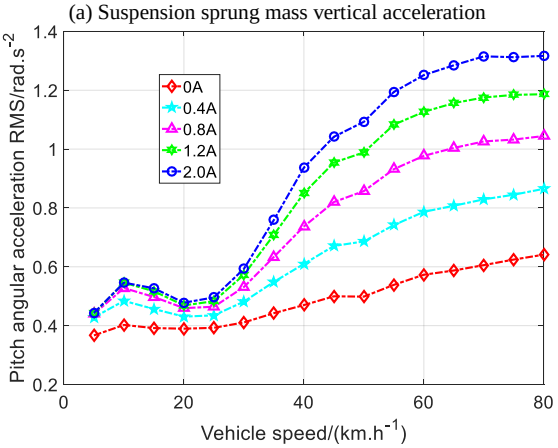

(b) Vehicle pitch angle acceleration

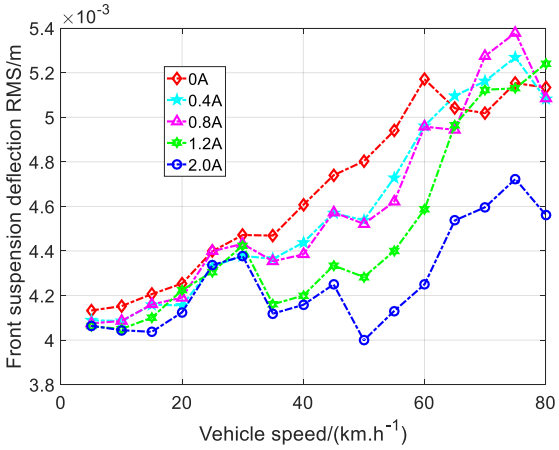

(c) Front suspension deflection

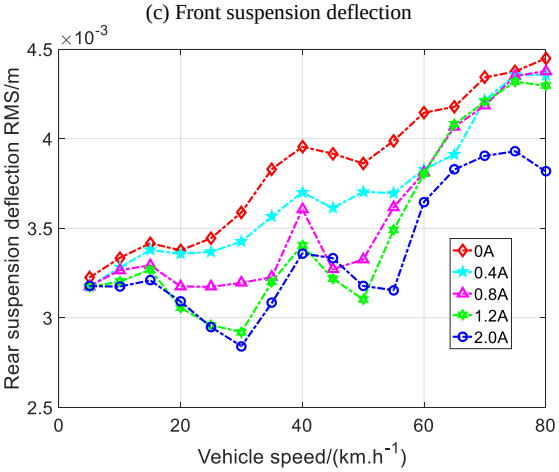

(d) Rear suspension deflection

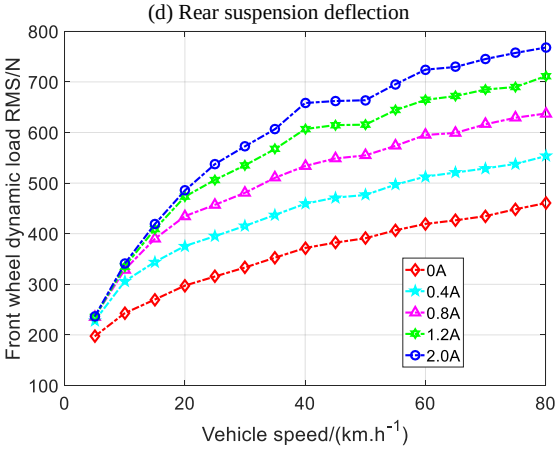

(e) Front tire dynamic load

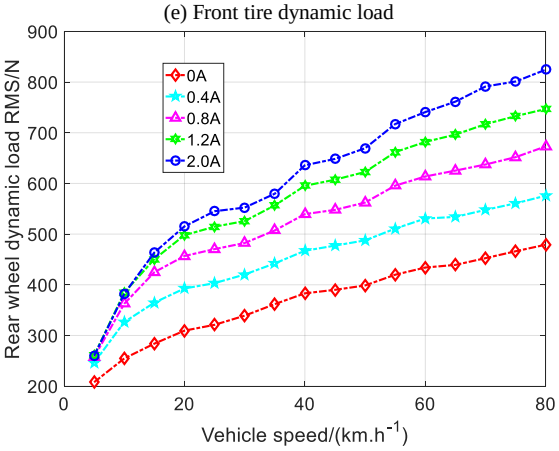

(f) Rear tire dynamic load

Fig.12. Output characteristic of the 4 DOF MR semi-active suspension

(1) Vertical Acceleration of Sprung Mass

The RMS value of the vehicle's vertical acceleration

increases with excitation current at a constant speed, with significant variation between 20 km/h and 40 km/h. At a constant excitation current, the RMS value increases with speed from 5 km/h to 25 km/h, decreases between 25 km/h and 60 km/h, and rises again from 60 km/h to 80 km/h.

(2) Pitch Angular Acceleration

The RMS value of pitch angular acceleration increases with excitation current at a constant speed, showing little variation between 15 km/h and 25 km/h. At a constant current, the RMS value shows an upward trend as speed increases.

(3) Deflection of Suspension

For the front suspension, the RMS deflection generally decreases with increasing excitation current at a constant speed, with larger variation at higher speeds. At a constant current, the RMS deflection of the front suspension generally increases with speed. For the rear suspension, the RMS deflection similarly decreases with increasing current, showing greater variation at medium speeds. At a constant current, the rear suspension deflection generally increases with speed.

(4) Dynamic Load on Tires

The RMS dynamic load on the front and rear tires increases with excitation current at a constant speed. At a constant current, the dynamic load on both front and rear tires increases with speed.

C. Numerical Simulation Analysis of Semi-Active Control

Skyhook control, a common strategy for semi-active suspensions, is chosen to assess the behavior of the 4-DOF semi-active suspension system. For comparison, a non-actuated MR damper is used as the passive suspension benchmark. The mathematical expression of the skyhook control law is given below [26].

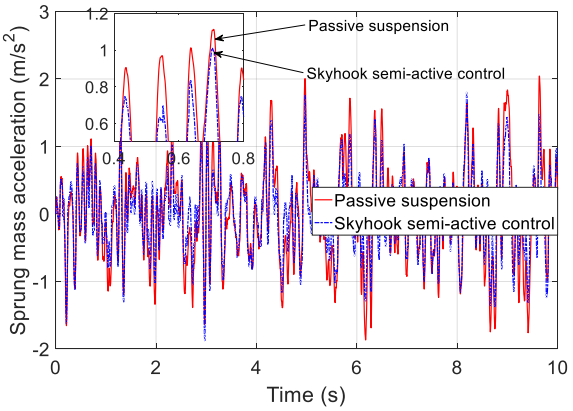

(a) Suspension sprung mass vertical acceleration

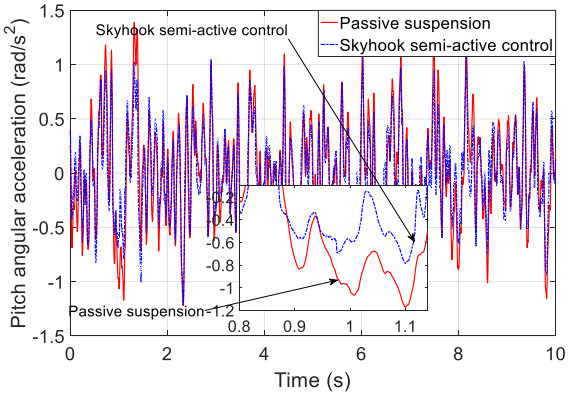

(b) Vehicle pitch angle acceleration

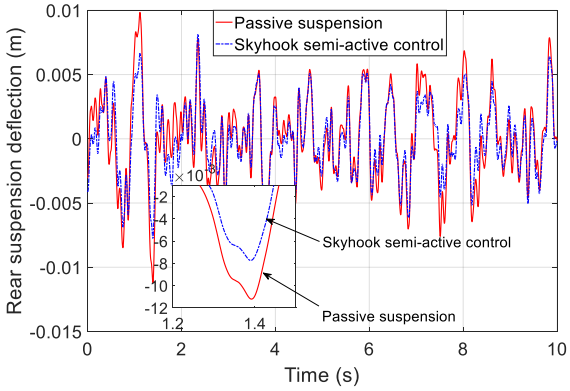

(c) Rear suspension deflection

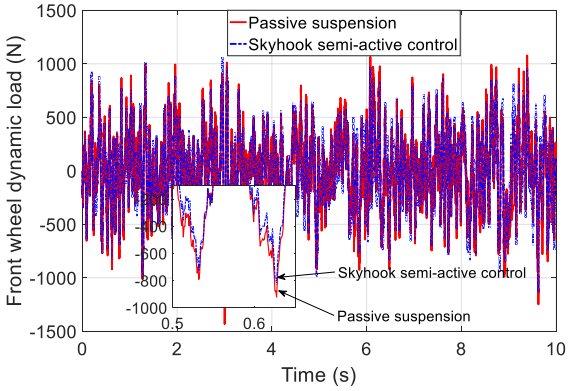

(d) Front tire dynamic load

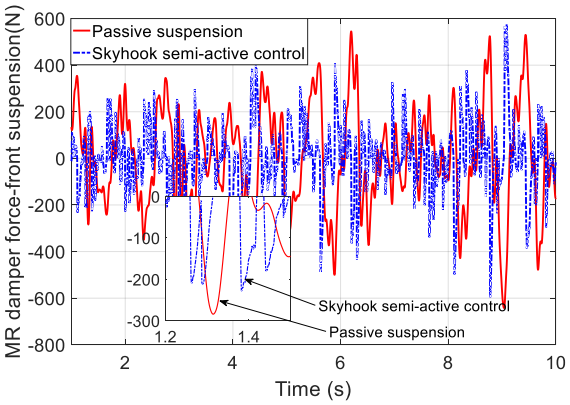

(e) Output force of MR damper

Fig.13. Output characteristics of the 4-DOF suspension under Skyhook semi-active control

$$F_{sky}=\begin{cases} F_{\max} & \dot{z}_s(\dot{z}_s-\dot{z}_u)\geq 0 \quad and \quad F_{sky}>F_{\max} \\ F_{\max} & \dot{z}_s(\dot{z}_s-\dot{z}_u)\geq 0 \quad and \quad F_{sky}\leq F_{\max} \\ 0 & \dot{z}_s(\dot{z}_s-\dot{z}_u)<0 \end{cases} \tag{12}$$

where $\dot{z}_s$ and $\dot{z}_u$ represent the velocities of the sprung and un-sprung masses of the suspension, respectively, and F_{sky} and $F_{\max}$ are the output and maximum output forces of the MR damper, respectively.

A random excitation at 40 km/h is used as the input for the suspension system. Figure 13 shows representative suspension output responses under different control strategies.

Figure 13 shows that applying skyhook control to the 4-DOF semi-active suspension produces a significant improvement on the output characteristics of both the sprung mass acceleration and pitch angle acceleration versus the passive suspension. Additionally, the suspension's dynamic deflection is slightly reduced, with no major increase in wheel dynamic loads or the damper's output force.

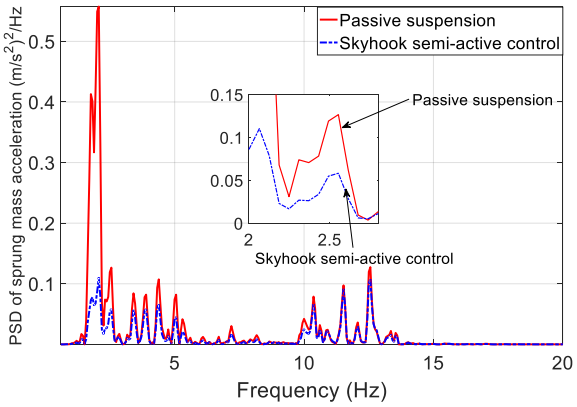

(a) PSD of suspension sprung mass vertical acceleration

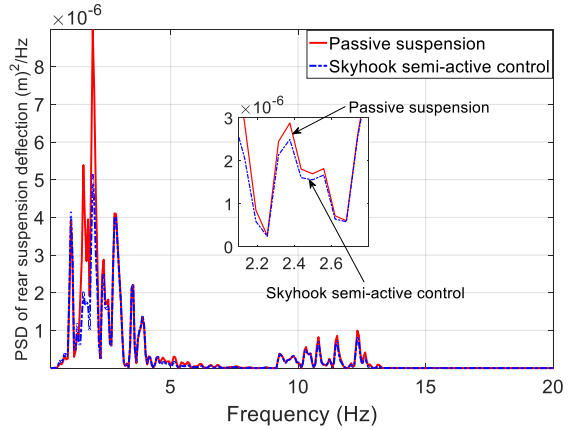

(b) PSD of rear suspension deflection

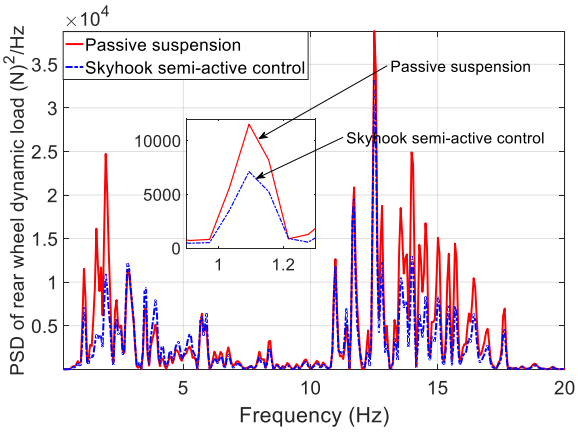

(c) PSD of front tire dynamic load

Fig.14. PSD of the 4-DOF suspension output characteristics under Skyhook semi-Active control

The PSD curves for the vertical acceleration of the sprung mass, the dynamic deflection of the rear suspension, and the dynamic load on the front tire are presented in Figure 14. Figure 14 illustrates that the random road excitation model, along with the 4-DOF MR semi-active suspension model developed in this study, supports research into semi-active control of MR vehicle suspensions.

Figure 14(a) shows that applying skyhook control to the semi-active suspension significantly reduces sprung mass acceleration near the first-order resonance peak. Skyhook control similarly reduces sprung mass acceleration near the second-order resonance peak, though the effect is notably weaker than at the first-order peak. The PSD curves for the suspension's dynamic deflection and the tire's dynamic load suggest that applying skyhook control to the MR semi-active suspension reduces both dynamic deflection and tire load across most excitation frequencies. Overall, applying skyhook control to the MR semi-active suspension effectively enhances ride comfort and stability in handling. These findings further confirm the effectiveness and broad application potential of the proposed 4-DOF semi-active suspension control model.

VI. Conclusion

This study investigated a 4-DOF semi-active vehicle suspension system utilizing a double-ended rod magneto-rheological (MR) damper. The key findings are:

(a) Road Excitation Modeling

A time-domain simulation model for road random excitation was created using filtered white noise and a first-order Padé approximation. The model's PSD curve complies with national standards, confirming its feasibility and applicability.

(b) Rheological Properties and Damper Development

The chosen MR fluid exhibited shear stress ranging from 0.02 kPa to 45 kPa under different magnetic fields, confirming its suitability for MR dampers. The developed double-ended rod MR damper demonstrated an increase in damping force with rising excitation current, indicating distinct variable damping characteristics and excellent controllability. The control model derived from experimental data confirmed high accuracy.

(c) Dynamic Modeling and Simulation

A dynamic model of the 4-DOF semi-active suspension system, integrated with the developed MR damper, was established. MATLAB/Simulink simulations examined the suspension's response under varying vehicle speeds and excitation currents, revealing their significant effects on output characteristics. The performance metrics of the 4-DOF semi-active suspension system increase with the rise in vehicle speed and excitation current, exhibiting clear regularity and controllability.

(d) Verification of Semi-Active Control through Simulation

To further validate the proposed random road excitation model and the 4-DOF semi-active suspension model, a vibration control simulation was performed using the standard skyhook semi-active control strategy. Time-domain and frequency-domain simulation results show that, compared to passive suspension systems, applying the skyhook semi-active control strategy to the 4-DOF suspension model significantly reduces sprung mass acceleration, pitch angle acceleration, dynamic deflection, and tire dynamic load over most time periods and excitation frequencies. Overall, skyhook control based on the proposed 4-DOF suspension model effectively improves ride comfort and handling stability. This further validates the effectiveness of the proposed random road excitation model and 4-DOF suspension model, highlighting their broad applicability in dynamic matching of suspension stiffness and damping, as well as in developing and testing semi-active control strategies for vehicle suspensions.

Overall, this study demonstrates the effectiveness of the double-ended rod MR damper in enhancing vehicle suspension performance. The comprehensive analysis and modeling provide a solid theoretical foundation for advancing

semi-active suspension technologies, addressing the evolving needs of intelligent vehicle systems.

REFERENCES

[1] C. Zhang, R. C. Jiang, "Research on Collaborative Optimization of Vehicle Ride Comfort and Handling Stability," Journal of Machine Design, vol. 39, no.S2, pp46-50, 2022.

[2] F. N. Cai, H. L. Zhao, B. B. Sun, L. Sun, "Design Optimization of FSAE Car Steering System," IAENG International Journal of Applied Mathematics, vol. 53, no.4, pp1648-1656, 2023.

[3] A. Bawa, and M. N. Nwohu, "Investigating the Penetration Rate of Electric Vehicle in Developing Countries: Nigeria as A Case Study," Lecture Notes in Engineering and Computer Science: Proceedings of The International Multi Conference of Engineers and Computer Scientists 2023, 5-7 July, 2023, Hong Kong, pp105-109.

[4] L. X. Zhang, N. F. Li, G. Q. Liang, "Research on Smooth Skyhook Control Strategy of Semi-active Suspension with Continuously Adjustable Damping," Noise and Vibration Control, vol. 43, no.2, pp169-173, 2023.

[5] K. Wu, "Research on Machine Learning Algorithm for Intelligent Suspension," Master's dissertation, Qingdao University of Technology, Qingdao, China, 2022.

[6] P. He, J. H. Chen, J. Xu, "Experimental Study on Performance of Magnetorheological Dampers," Noise and Vibration Control, vol. 43, no.2, pp278-284, 2023.

[7] Y. C. Ge, G. Liu, "Design and Simulation of Composite Energy Regenerative Magnetorheological Shock Absorber," Machine Tool & Hydraulics, vol. 51, no.6, pp163-170, 2023.

[8] C. L. Shen, X. Y. Ma, J. YU Jing, Y. Z. Ye, Y. B. Yue, Z. H. Gao, "A Review of the Development Status of Intelligent Materials for Vehicles," Journal of Jilin University (Engineering and Technology Edition), vol. 53, no. 7, pp1-19, 2023.

[9] S. K. Lohit, K. Hemanth, H. Kumar, K. V. Gangadharan, "Experimental and Analytical Studies on Magnetorheological Damper," Applied Mechanics and Materials, vol. 854, pp127-132, 2016.

[10] K. Kecik, A. Mitura, D. Sado, J. Warminski, "Magnetorheological Damping and Semi-Active Control of an Auto Parametric Vibration Absorber," Meccanica, vol. 49, no. 8, pp1887-1900, 2014.

[11] J. H. Fu, Y. K. Yin, J. T. Su, M. Chen, Z. M. Chen, B. Chen, "Research Review of Automotive Powertrain Magnetorheological Mount," Journal of Chongqing University of Technology (Natural Science), vol. 37, no. 6, pp29-38, 2023.

[12] Q. Zhao, P. D. Wang, L. Luo, J. Li, "Establishment of Simulink Model for Road Excitation and its Application," Science Technology and Engineering, vol. 18, no. 1, pp128-132, 2018.

[13] Q. Zhao, W. Wang, J. Li, C. X. Zhang, "Modeling and Simulation of Time Domain for Automotive Ride Comfort based on a Filtered White Noise," Science Technology and Engineering, vol. 16, no. 27, pp283-287, 2016.

[14] Q. Zhao, W. Wang, L. Luo, L. L. Zheng, J. Li, "Modeling and Simulation of Time Domain for Car Ride Comfort based on a Space Model," Science Technology and Engineering, vol. 17, no. 4, pp99-104, 2017.

[15] Q. Zhao, K. Yang, L. Luo, J. Li, "Modeling and Frequency Domain Simulation of Ride Comfort for Six-axle Tractor Semi-trailer," Science Technology and Engineering, vol. 17, no. 36, pp117-123, 2017.

[16] F. Kong, H. J. Liao, R. J. Han, Y. Zhang, X. Hong, "A semi Analytical Method for Non Stationary Response Determination of Nonlinear Systems Subjected to Combined Excitation," Journal of Vibration Engineering, vol. 2023, no. 3, pp1-10, 2023.

[17] D. B. Liu, Y. Wang, B. W. Li, Z. F. Yi, L. Zhang, H. Li, "An Improved Precise Integration Single-step Method for Nonlinear Dynamic Equations," Journal of Vibration and Shock, vol. 41, no. 5,pp182-188, 2022.

[18] X. G. Liu, "Research and Optimization on Dynamic Characteristics of Bogie Frame," Master's dissertation, Southwest Jiaotong University, Chengdu, China, 2017.

[19] X. X. Bai, X. C. Deng, S. Shen, "Controllability Calibration of Magnetorheological Shock Absorbers," Journal of Hefei University of Technology (Natural Science), vol. 44, no. 8, pp1026-1032, 2021.

[20] G. Q. Liang, T. Zhao, J. C. Lv, Y. T. Wei, "Magnetorheological Damper Extreme High and Low Temperature Characteristics and Variable Temperature Forward and Reverse Models," China Journal of Highway and Transport, vol. 35, no. 10, pp280-289, 2022.

[21] S. C. Song, Y. P. Luo, Q. B. Fang, S. C. Wang, "Research Advances in Effect of Magnetorheological Fluid Components on Sedimentation," Chemistry, vol. 86, no. 1, pp78-82, 2023.

[22] B. Y. Liu, "Design and performance study on MR damper of hole-type," Master's dissertation, Civil Aviation University of China, Tianjin, China, 2015.

[23] W. Liu, S. J. Sun, F. C. Pang, L. L. Wang, "Analysis of QC/T491-2018 Automobile Shock Absorber Standard," Automobile Applied Technology, vol. 45, no. 18, pp268-270, 2019.

[24] J. Hernadi, "Numerical and Experimental for Optimal Sensor Location in Lumped and Distributed Parameter System," IAENG International Journal of Computer Science, vol. 49, no.4, pp1055-1062, 2022.

[25] F. Yu and Y. Lin, "Vehicle system dynamics," China Machine Press, Beijing, 2005.

[26] W. F. Li, X. F. Ge, M. Y. Liang, X. Deng, "Magneto-rheological variable damping and variable stiffness torsional vibration control of powertrain transmission," Journal of Mechanical Science and Technology, vol.37, no.8, pp1-14, 2023.

Xin-feng Ge received his B. Sc. And M. Sc. degrees in mechanical engineering from Henan Agricultural University, China in 2002 and 2005, respectively. He is currently a professor in School of Electrical and Mechanical Engineering, Xuchang University, Xuchang, 461000, China. (phone:+8618539037370; e-mail: gexf@xcu.edu.cn). His main research interest is vibration control and intelligent manufacturing.

Wen-feng Li received his Ph. D. degree in mechanical engineering from Chongqing University, China in 2021. He is currently a lecturer in School of Electrical and Mechanical Engineering, Xuchang University, Xuchang, 461000, China. (e-mail: 418974195@qq.com). His main research interest is intelligent mechanical mechanisms and vibration control.

Man-ying Liang is currently a lecturer in School of Electrical and Mechanical Engineering, Xuchang University, Xuchang, 461000, China. (e-mail: 1324981596@qq.com). His main research interest is vibration control and intelligent manufacturing.

Shen-shen Zhang is currently an undergraduate student in School of Electrical and Mechanical Engineering, Xuchang University, Xuchang, 461000, China. (e-mail: 2073931517@qq.com).

Kai-yang Huo is currently an undergraduate student in School of Electrical and Mechanical Engineering, Xuchang University, Xuchang, 461000, China. (e-mail: 1468523752@qq.com).